

Energy Management Control Strategy for Standalone DC Microgrids

Sai Navesh Manchem¹, Muralidhar Kalal²

M.Tech Student Scholar, Department of EEE, Malla Reddy Engineering College, Hyderabad, Telangana, India¹

Assistant Professor, Department of EEE, Malla Reddy Engineering College, Hyderabad, Telangana, India²

Abstract: As the demand of Electricity is increasing day by day and is already more than the production of Electricity whereas reserves of fossil-fuel are depleting, there is a strong need to shift for other sources which are renewable energy sources. Regarding this, DC micro grids and their energy management of these renewable energy sources have gained more importance which is discussed in this paper. The main objective of the proposed system is to provide uninterrupted power supply to the load systems which are located at isolated sites of remote and rural areas. The proposed system mainly deals with implementation of Energy Management System (EMS) to DC microgrid using maximum power point tracking (MPPT) algorithm. A coordinated and multivariable EMS is proposed that employs a wind turbine and a photovoltaic array as controllable generators by adjusting the pitch angle and the switching duty cycles and a storage system consisting of batteries. In order to realize constant current, constant voltage (IU) charging regime and increase the life span of batteries, the proposed EMS require being more flexible with the power curtailment feature. The proposed strategy is developed as an online nonlinear model predictive control (NMPC) algorithm based on individual MPPTs of the system. The entire designed system is modeled and simulated using MATLAB/Simulink Environment.

Key words: Battery Management, Maximum Power Point Tracking (MPPT), Nonlinear Model Predictive Control (NMPC), Power Sharing, and Voltage Regulation.

I. INTRODUCTION

Microgrids are new key elements of modern power grids that improve the grids capability of hosting renewable energy and distributed storage systems [1] consisting of ac and dc loads [2]. The near future distribution networks will consist of several interconnected microgrids which will locally generate, consume, and store energy [3]. A microgrid may be operated as an extension of the main grid, i.e., grid-connected, or as a standalone network with no connection to the grid. Standalone dc microgrids have some distinct applications in avionic, automotive, or marine industries, as well as remote rural areas. Due to substantial generation and demand fluctuations in stand-alone green micro-grids, energy management strategies (EMSSs) are becoming essential for the power sharing purpose and regulating the microgrids voltage. The classical EMSSs track the maximum power points (MPPs) of wind and PV branches independently and rely on batteries, as slack terminals, to absorb any possible excess energy. However, in order to protect batteries from being overcharged by realizing the constant current, constant voltage (IU) charging regime as well as to consider the wind turbine operational constraints, more flexible multivariable and non-linear strategies, equipped with a power curtailment feature are necessary to control microgrids.

The stability of a dc microgrid is measured in terms of the stability of its dc bus voltage level which is one of the main control objectives [4]. The grid voltage source converters (G-VSCs) are the primary slack terminals to regulate the voltage level of grid-connected microgrids. Battery banks, on the other hand, are effective slack

terminals for standalone microgrids [5]. The curtailment strategies [6] of the battery bank which cannot absorb the excess generation restrict the batteries charging rate by the maximum absorbing power; however, the maximum charging current must also be limited. Furthermore, they do not curtail the power of each generator in proportion to its rating. In order to prevent over-stressing conditions and circulating currents between generators [7], load demands need to be shared between all slack DGs in proportion to their ratings [8]. However, standalone dc microgrids are usually located in small-scale areas where the power sharing between DGs can be managed by centralized algorithms which are less affected by two issues: 1) batteries in charging mode are nonlinear loads causing distortions to the grid voltage; and 2) the absolute voltage level of a standalone microgrid is shifted as the result of the load demand variation.

A number of phenomena affect the batteries operation during the charging mode [9]: 1) applying high charging currents, the batteries voltages quickly reach to the gassing threshold; 2) the internal resistor and hence power losses and thermal effects increase at high SOC levels; and 3) batteries cannot be fully charged with a constant high charging current and also restricts the maximum attainable SOC that leads to unused capacities [10]. However, since batteries act as nonlinear loads during the charging mode, it does not necessarily limit the charging currents. Depending on the proportion of the power generation to the load demand ratio within standalone DC microgrids, three cases are envisaged: 1) power generation and load demand are balanced; 2) load demand exceeds power

generation causes dc bus voltage to drop in absence of any load shedding; and 3) power generation is higher than load demand leads batteries to be overcharged and bus voltage to climb. This study focuses on case 3) in which the generated power must be curtailed if it violates the batteries charging rates or if batteries are fully charged. In contrast to the strategies available in which renewable energy systems (RESs) always operate in their MPPT mode, the proposed multivariable strategy uses a wind turbine and a PV array as controllable generators and curtails their generations if it is necessary. The proposed EMS is developed as an online novel NMPC strategy that continuously solves an optimal control problem (OCP) and finds the optimum values of the pitch angle and three switching duty cycles. It simultaneously controls four variables of microgrids: 1) power coefficient of the wind turbine; 2) angular velocity of the wind generator; 3) operating voltage of the PV array; and 4) charging current of the battery bank. It is shown that employing new available nonlinear optimization technique and tools, the computational time to solve the resulting NMPC strategy is in permissible range. Unlike dump load-based strategies that only protect the battery from over charging, the proposed strategy implements the IU charging regime that helps to increase the batteries life span.

II. SYSTEM DESCRIPTION AND MODELLING

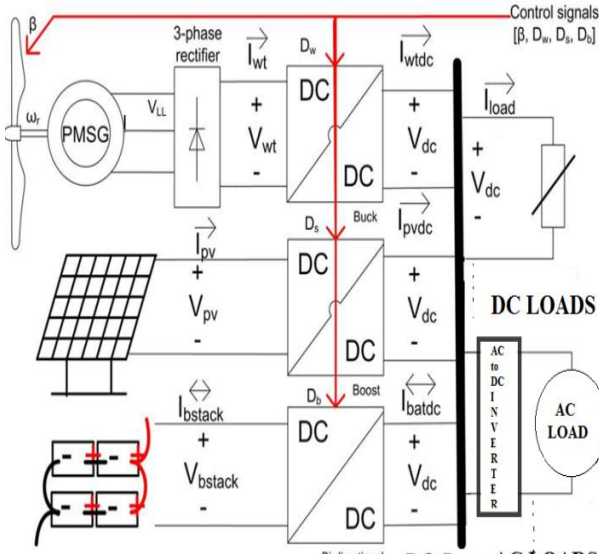


Fig.1. Topology of a small-scale and standalone dc microgrid with connected loads.

Fig.1. shows the Topology of a small-scale and standalone dc microgrid with connected loads. The mathematical model of stand-alone green dc microgrids is described as hybrid differential algebraic equations (hybrid DAEs). The below figure Fig.2 summarizes a modified version of the proposed model. Since this paper focuses on the case in which there is an excess power greater than or equal to the maximum possible absorbing rate of the battery bank the following notations are used to model the standalone dc.

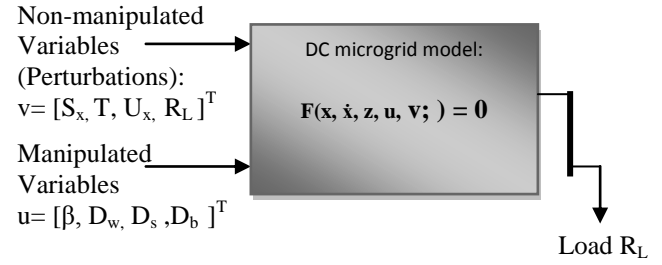


Fig 2 Modified version of the system model

$$X = [I_f, Q_{act}, \omega_r]^T \quad (1a)$$

$$z = [I_{pv}, V_{pv}, I_{pvdc}, I_{bat}, I_{batdc}, V_{batdc}, I_{wt}, V_{wt}, I_{wtdc}, T_e, T_m, \lambda, C_p, SOC, I_{load}, V_{dc}]^T \quad (1b)$$

$$F(x, \dot{x}, z, u, v) = \begin{bmatrix} f_1(x, \dot{x}, z, u, v) \\ f_2(x, \dot{x}, z, u, v) \\ \vdots \\ f_{24}(x, \dot{x}, z, u, v) \end{bmatrix} = 0 \quad (1c)$$

Where F is a set of implicit differential and algebraic functionals f_i for $i \in [1, 2, 3 \dots 24]$. The first two constraints f_1 and f_2 are due to the fact that in standalone dc microgrids the sum of the generated, stored, and consumed powers is always zero:

$$f_1 = V_{dc} (I_{pvdc} + I_{wtdc} + I_{batdc} + I_{load}) \quad (2a)$$

$$f_2 = V_{dc} - I_{load} R_L \quad (2b)$$

A. Wind Branch

Wind turbines (WTs) convert the kinetic energy of wind to mechanical power. In order to generate the maximum power by a WT at variable wind speed, it is necessary to employ a maximum power point tracking (MPPT) control strategy [11]. A wind turbine can be connected to an electrical generator directly or through a gear-box. In order to convert the three-phase output of a PMSG to dc voltage, it is essential to deploy a three-phase rectifier. A general structure, which consists of a full-bridge diode rectifier connected in series to a dc-dc converter, is common due to lower cost.

Performance of the wind turbines is measured as the power coefficient curve with respect to the tip speed ratio and pitch angle. Equation (3) shows the power coefficient curve of three-blade wind turbines

$$f_3 = C_{p,norm} - \frac{1}{C_{p,max}} \times \left(C_1 \left(\frac{C_2}{\lambda_i} - C_3 \beta - C_4 \right) \exp \left(-\frac{C_5}{\lambda_i} \right) + C_6 \lambda \right) \quad (3a)$$

$$f_4 = \lambda - \frac{Rad \times \omega_r}{u_x} \quad (3b)$$

$$f_5 = \lambda_i - \left(\frac{1}{\lambda_i + 0.08\beta} - \frac{0.035}{\beta^3 + 1} \right)^{-1} \quad (3c)$$

Where λ and β , respectively, are the tip speed ratio and pitch angle. Rad is the radius of the blades and $C_{p,max}$ is the maximum achievable power coefficient at the optimum tip speed ratio of λ_{out} .

The below equation (4) presents the connected PMSG generator.

$$\mathbf{f}_6 = \frac{d\omega_r}{dt}(\mathbf{t}) \frac{1}{J} (\mathbf{T}_e - \mathbf{T}_m - \mathbf{F}\omega_r) \quad (4a)$$

$$\mathbf{f}_7 = \mathbf{T}_e \times \omega_r - \mathbf{I}_{wtdc} \times \mathbf{V}_{dc} \quad (4b)$$

$$\mathbf{f}_8 = -\mathbf{T}_m \times \omega_r - \left(C_{p,norm} \left(\frac{U_Z}{U_{Z,base}} \right)^3 P_{nom} \right) \quad (4c)$$

Energy management strategies of microgrids must estimate the dc bus voltage level deviation from its set point in about every 5–10 sec. It means that except the angular velocity of the generator (4a) all other fast voltage and current dynamics can be ignored. It is also assumed that there are no mechanical and electrical losses through the power train and therefore the electromagnetic power given by (4b) is equal to the output electrical power of the wind branch. Equation (4c) shows that the PMSG is connected directly to turbine, which rotates at low speed, and therefore needs to have multiple pole pairs P. Hence, the electrical frequency is P times faster than the mechanical angular velocity ω_r . The shaft inertia J (Kg.m^2) and the combined viscous friction coefficient F (N.m.s) of PMSG are given by the manufacturers. For energy management strategies, the average model of the buck converter is replaced with the steady-state equations for the continuous conduction mode (CCM).

$$\mathbf{f}_9 = \mathbf{V}_{dc} - D_w \mathbf{V}_{wt} \quad (5a)$$

$$\mathbf{f}_{10} = \mathbf{I}_{ut} - D_u \mathbf{I}_{wtdc} \quad (5b)$$

Where D_w is the switching duty cycle of the converter. The average dc output voltage of the rectifier \mathbf{V}_{wt} in presence of the non-instantaneous current communication is calculated as below.

$$\mathbf{V}_{wt} = 1.35 \mathbf{V}_{LL} - \frac{3}{\pi} \omega_e L_s I_{wt} \quad (6)$$

Then considering the r.m.s value of line to line voltage the dc output current of wind turbine is given by is given by

$$\mathbf{f}_{11} = \mathbf{I}_{wtdc} - \frac{\pi}{3P\omega_r L_s D_w} \left\{ \frac{1.35\sqrt{3}P\Psi\omega_r}{\sqrt{2}} - \frac{\mathbf{V}_{dc}}{D_u} \right\} \quad (7)$$

B. Battery Branch

There are different types of batteries applicable to the backup/storage purposes across microgrids. Among all the lead-acid batteries have some advantages for hybrid renewable energy system (HRES) applications. Lead-acid batteries are widely available in many sizes and are appropriate for small to large applications. Furthermore, the normalized cost of this type of batteries is reasonable and it is mature in concepts, mathematical model and technology. In fact, the performance characteristics of lead-acid batteries are well understood and modelled.

The charging operation of a lead acid battery bank, consisting of $N_{batp} \times N_{bats}$ batteries is modelled [12] as below.

$$\mathbf{f}_{12} = \frac{\mathbf{V}_{bstack}}{N_{bats}} - \mathbf{V}_0 + R_{bat} \frac{I_{bstack}}{N_{batp}} + \frac{P_1 C_{max}}{C_{max} - Q_{act}} Q_{act} + \frac{P_1 C_{max}}{Q_{act} + 0.1 C_{max}} I_f \quad (8a)$$

$$\mathbf{f}_{13} = \frac{dQ_{act}}{dt}(\mathbf{t}) - \frac{1}{3600} \left(\frac{I_{bstack}(\mathbf{t})}{N_{batp}} \right) \quad (8b)$$

$$\mathbf{f}_{14} = \frac{dI_f}{dt}(\mathbf{t}) + \frac{1}{T_s} \left(I_f - \frac{I_{bstack}}{N_{batp}} \right) \quad (8c)$$

$$\mathbf{f}_{15} = \mathbf{V}_{bstack} - \frac{\mathbf{V}_{dc}}{(1 - D_b)} \quad (8d)$$

$$\mathbf{f}_{16} = \mathbf{V}_{bstack} - (1 - D_b) \mathbf{I}_{batdc} \quad (8e)$$

$$\mathbf{f}_{17} = SOC - \left\{ 1 - \frac{Q_{act}}{C_{max}} \right\} \quad (8f)$$

Where \mathbf{V}_{bstack} , I_{bstack} , and SOC are, respectively the voltage, current, and state of charge of the battery bank. I_f is the filtered value of the battery current with the time constant of T_s and Q_{act} is the actual battery capacity. The experimental parameter P_1 requires being identified for each type of battery while the maximum amount of the battery capacity, C_{max} , internal resistor of battery, R_{bat} , and the battery constant voltage, V_0 , are given by manufacturers. By ignoring the discharging mode of the battery bank operation, the bi-directional converter acts as a boost-type converter [(8d), (8e)].

C. Solar Branch

PVs are among the popular renewable energy components to harvest solar energy. A PV cell, as the fundamental PV element, is a P-N junction that converts solar irradiance to the electrical energy. Normally, manufacturers provide PV modules, also known as PV panels, which consist of several PV cells connected together in series. A PV cell is a non-linear component that its operation is characterised by a set of current-voltage curves at different insolation levels and junction temperatures.

The equivalent electrical circuit of the PV module is used to mathematically model the solar branch, consisting of a PV array and a boost converter [13]. The below equations shows the characteristic equations of a PV array, consisting of $N_{pvp} \times N_{pvs}$ PV modules:

$$\mathbf{f}_{18} = I_{pv} - I_{ph} + I_0 \left\{ \exp \left(\frac{V_{pv} + \frac{N_{pvs}}{N_{pvp}} R_s I_{pv}}{n_d N_s} \frac{q \times N_{pvs}}{K T_c} \right) - 1 \right\} + \frac{V_{pv} + \frac{N_{pvs}}{N_{pvp}} R_s I_{pv}}{\frac{N_{pvs}}{N_{pvp}} R_{sh}} \quad (9a)$$

$$\mathbf{f}_{19} = I_{ph} - N_{pvp} \times \left(\frac{R_s + R_{sh}}{R_{sh}} I_{sc,stc} + K_I (T_c - T_{c,stc}) \right) \frac{S}{S_{stc}} \quad (9b)$$

$$f_{20} = I_0 - N_{pvp} \times \frac{I_{sc,stc} + K_f(T_c - T_{c,stc})}{\exp\left(\frac{V_{oc,stc} + K_V(T_c - T_{c,stc})}{n_d N_s} \frac{q}{K T_c}\right) - 1} \quad (9c)$$

Where I_{ph} denotes the photocurrent and I_0 is the diode reverse saturation current. R_s and R_{sh} , respectively, are the series and parallel equivalent resistors of each PV module. Similar to the wind branch, the average model of the boost converter is replaced with the steady-state equation.

$$f_{21} = V_{pv} - (1 - D_s) V_{dc} \quad (10a)$$

$$f_{22} = I_{pvdc} - (1 - D_s) I_{pv} \quad (10b)$$

D. Maximum Power Point Tracking

Maximum power point tracking (MPPT) is a technique used commonly with wind turbines and photovoltaic (PV) solar systems to maximize power extraction under all conditions. The MPPT technique is also useful for the operation of battery. Depending upon the MPPT technique charging and discharging modes of operations of batteries are controlled. It is useful in protecting the battery from over charging, and to implement the IU charging regime of the battery that helps to increase the life span of batteries.

The output power induced by the pv modules and wind turbine are influenced by number of factors which are solar radiation, temperature, wind speed etc. To maximize the power output from the system it is necessary to track the maximum power points of the individual energy sources. There are several methods to track the mpp's of the system among them P&O is the commonly used method.

E. Power Conversion

In order to supply different types of variable dc and variable ac loads connected to the isolated standalone dc micro grid, and depending on the energy supplying sources and storage systems it is necessary to convert the energy to maintain the dc bus voltage regulation. Depending upon the load connected and the energy sources the energy conversion is either DC-DC or DC-AC [14]. And only the AC-DC conversion is needed at wind turbine through bridge rectifier to connect dc bus.

1) Dc-Dc Converters:

DC-DC converter is an electrical circuit whose main application is to transform a dc voltage from one level to another level. It is similar to a transformer in AC source, it can able to step the voltage level up or down. The variable dc voltage level can be regulated by controlling the duty ratio (on-off time of a switch) of the converter. Dc-dc converters are normally implemented based on the switching-mode circuit technology containing at least one energy storage and a transistor-based power-pole. However, in ideal cases, a single-pole double-throw switch can also be used for simulation purpose [15]. Here we are mainly using 3 types of converters. They are 1) Boost converter 2) Buck converter 3) Bidirectional converters.

The boost-type converter scales up its input voltage, which is used for PV array system, a buck-type converter

provides lower voltage than the input voltage, which is used for wind turbine. Unlike the boost and buck converters, bi-directional converter dictates the instantaneous current flow to be unidirectional. In such a converter a complementary control signal allows the current to flow in either direction. This is connected to battery for the purpose of charging and discharging the battery based on the surplus and deficit of the power respectively.

2) Dc-Ac and Ac-Dc Conversion:

The ac-dc conversion is needed at wind turbine through bridge rectifier to connect dc bus. And the dc-ac conversion is performed at the terminal slack side of the dc bus bar to supply the ac loads as the majority of the industrial avionic application loads are in ac nature. The dc-ac conversion is performed through bridge rectifier which operation is controlled by the pwm technique.

A state-space averaging approach to model a dc-dc converter is implemented which suggests two states, I_l and V_c for the continuous conduction mode (CCM) in which the instantaneous inductor current I_l is always greater than zero. According to the proposed approach, there is a set of two distinct state-space systems to model two states of switch operation and the overall state-space model of the converter is a weighted average of these two models. The weighting factor is the duration of time that converter remains in each state.

While state-space averaging approach is simple to analyse and implement, it does not model the hybrid nature of converters. One-level dc-dc converters work in two different modes of operation with respect to the value of discrete state S_d . Defining the same state vector as above, i.e. $X^T = [I_l \ V_c]^T$, dc-dc converters can be modelled as hybrid systems. It presents an affine state space model coupled with a linear output equation for each modes of operation.

III. CONTROLLER DESIGN

A. Nonlinear Model Predictive Control (NMPC)

Non-linear model predictive control (NMPC) strategies are inherently multivariable and handle constraints and delays. In this thesis, the EMS is developed as a NMPC strategy to extract the optimal control signals, which are duty cycles of three DC-DC converters and pitch angle of a wind turbine.

1) Optimal Control Problems (OCPS):

OCPs, make explicit use of the system model, given by the below functions in order to find an optimal control law $u^*(.)$, which meets number of equality and inequality constraints. The term optimal here is defined with respect to a certain criterion that implies the control objectives. This criterion is specified with a cost functional J , consisting of the Lagrangian term \mathcal{L} and the terminal cost term \mathcal{M} . While the Lagrangian term indicates the cost function during the period of time T , the terminal cost penalizes final values.

$$\mathbf{u}^*(.) = \arg \underset{\mathbf{U}(.) \in \mathbb{R}^n}{\text{minimize}} \quad \mathbf{J}(\mathbf{x}(t), \mathbf{z}(t), \mathbf{u}(t), N) = \\ \int_t^{t+T} \mathcal{L}((\mathbf{x}(t), \mathbf{z}(t), \mathbf{u}(t))) dt + \mathcal{M}(\mathbf{x}(t), \mathbf{z}(t)) \quad (11a)$$

$$\text{s.t.: } \Phi((\mathbf{x}(t), \dot{\mathbf{x}}(t), \mathbf{z}(t), \mathbf{u}(t), \mathbf{v}(t))) = \mathbf{0} \quad (11b)$$

$$\mathcal{H}(\mathbf{x}(t), \mathbf{z}(t), \mathbf{u}(t)) < 0 \quad (11c)$$

$$\mathcal{R}(\mathbf{x}(T), \mathbf{z}(T)) = \mathbf{0} \quad (11d)$$

$$\mathbf{x}(t) = \mathbf{x}_0, \mathbf{z}(t) = \mathbf{z}_0 \quad (11e)$$

$$\forall t \in [t, t+T] \quad (11f)$$

$$\mathbf{x}(t) \in \Xi, \mathbf{z}(t) \in \mathbf{Z}, \mathbf{u}(t) \in \mathbf{Y} \quad (11g)$$

OCPs are open-loop strategies and are wrapped by a feedback loop to construct NMPC strategies. NMPC strategies, which are also called as the receding horizon control, continuously solve an OCP over a finite-horizon T using the measurements obtained at t as the initial values. Then the first optimal value is applied as the next control signal. Comparing with the conventional methods, NMPCs are inherently non-linear and multivariable strategies that handle constraints and delays.

There are three different techniques to discretize and solve OCPs of the above equations [16]: 1) dynamic programming method based on the Bellman's optimality principle; 2) indirect method based on the Pontryagin minimum principle; and 3) direct methods that convert OCPs into nonlinear optimization problems (NLPs) which are then solved by NLP solvers. In this paper, a direct method, named collocation discretization, is developed in CasADI environment. CasADI implements the automatic differentiation (AD) technique [17] to reduce the controller execution time. It employs the well-known interior point optimizer (IPOPT) tool to solve the resulting NLPs.

B. Control System

The proposed EMS successively gets the estimated system states, $\dot{\mathbf{x}}$, as inputs and calculates the optimal solution, $\mathbf{U}^*(.)$, as outputs. The external state estimator and the predictor of the non-manipulated variables are out of the scope of this paper. N step ahead predictions of the solar irradiance, wind speeds, and load demands are extracted either from a meteorological centre or an external predictor using autoregressive-moving-average (ARMA) technique. The bus voltage level of the microgrid, V_{dc} , is set externally and hence the developed controller can act as the secondary and primary levels of the hierarchical architecture.

The developed NMPC controller consists of three entities: 1) the dynamic optimizer that successively solves OCP at each sampling time h , defined in Table I; 2) the mathematical model, Φ , of the system to predict its behaviour; and 3) the cost function and constraints of the relevant OCP. The optimal pitch angle, $\bar{\beta}$, is applied as a set point to an inner closed-loop controller. Moreover, the optimal values of the switching duty cycles are applied to the pulse width modulators (PWMs) of the dc-dc converters.

TABLE I
 DESIGN PARAMETERS AND THE COMPUTATIONAL TIME OF
 THE DEVELOPED NMPC CONTROLLER

Parameter Name	Parameter Value
prediction horizon T (sec)	10
Sampling time h (sec)	5.0
No.of the discretization samples N	2
\bar{V}_{dc} (V)	
\bar{V}_{dc} (V)	48.0
Average Computational Time (sec)	2.066
Minimum Computational Time (sec)	0.628
Maximum Computational Time (sec)	3.565

Developing non-linear multivariable control strategies for stand-alone dc micro-grids to achieve five control objectives: i) supplying variable ac and dc loads; ii) regulating the dc bus voltage level; iii) charging batteries as close to IU regime as possible; iv) proportional power sharing between generators; v) tracking MPPs of wind and PV branches during normal operations.

1) Control Objectives:

Three aforementioned control objectives, i.e., dc bus voltage regulation, proportional power sharing, and implementing the IU regime to charge batteries, are formulated by two slack variables in (12)and (13) and the cost function J in equation (14).

$$f_{23} = \alpha_1 - (V_{dc} - \bar{V}_{dc}) \quad (12)$$

The permissible deviation of the dc bus voltage level V_{dc} from the specified set point \bar{V}_{dc} is defined by a slack variable α_1 in f_{23} . It is a design parameter set to $\pm 0.02\bar{V}_{dc}$ or equivalently ± 0.1 for a 48.0-volt dc bus:

$$f_{24} = \alpha_2 -$$

$$\left\{ \frac{I_{wtdc}V_{dc}}{P_{wt,norm}} \left(\frac{U_{z,base}}{\max(U_x, U_{x,base})} \right)^3 - \frac{I_{pvdc}V_{dc}}{P_{pv,norm}} \frac{S_{z,base}}{\max(S_x, S_{x,base})} \right\} \quad (13)$$

The permissible deviation from the proportional power sharing criterion is given in f_{24} as a slack variable α_2 . The design parameter α_2 is set to $\pm 1\%$ to increase the flexibility of the algorithm with the cost of a slight penalty. The generated powers are normalized with respect to the wind speed and insolation values, i.e., U_x and S_x . The IU charging regime is modelled as two cost functions for two separate cases:

$$J\{ x(n), z(n), u(n), N \} =$$

$$\sum_{k=n}^{n+N} \left\{ \beta_3 \left| \frac{V_{bstack}(k) - N_{bats} V_{gas}}{N_{bats} V_{gas}} \right|_2 + \beta_4 \left| \frac{V_{dc}(k) - \bar{V}_{dc}}{\bar{V}_{dc}} \right|_2 \right\} \\ + \left\{ \beta_3 \left| \frac{V_{bstack}(N) - N_{bats} V_{gas}}{N_{bats} V_{gas}} \right|_2 + \beta_4 \left| \frac{V_{dc}(N) - \bar{V}_{dc}}{\bar{V}_{dc}} \right|_2 \right\} \quad (14a)$$

$$J\{ x(n), z(n), u(n), N \} =$$

$$\sum_{k=n}^{n+N} \left\{ \beta_1 \left| \frac{1}{I_c} \left(\frac{I_{bstack}(k)}{N_{batp}} - \bar{I}_c \right) \right|_2 + \beta_2 \left| \frac{V_{dc}(k) - \bar{V}_{dc}}{\bar{V}_{dc}} \right|_2 \right\} \\ + \left\{ \beta_1 \left| \frac{1}{I_c} \left(\frac{I_{bstack}(N)}{N_{batp}} - \bar{I}_c \right) \right|_2 + \beta_2 \left| \frac{V_{dc}(N) - \bar{V}_{dc}}{\bar{V}_{dc}} \right|_2 \right\} \quad (14b)$$

When the battery voltage level is less than the gassing voltage, the proposed controller employs the first equation to charge the battery bank with the constant current \bar{I}_c . Once the battery voltage level exceeds the gassing voltage, the controller switches to second equation to maintain it below the gassing voltage V_{gas} and protect batteries from permanent damages. In order to prevent the dc bus voltage level from sticking at the upper or lower boundaries, the

IV. SIMULATION AND RESULTS

A. Matlab Simulation Circuit:

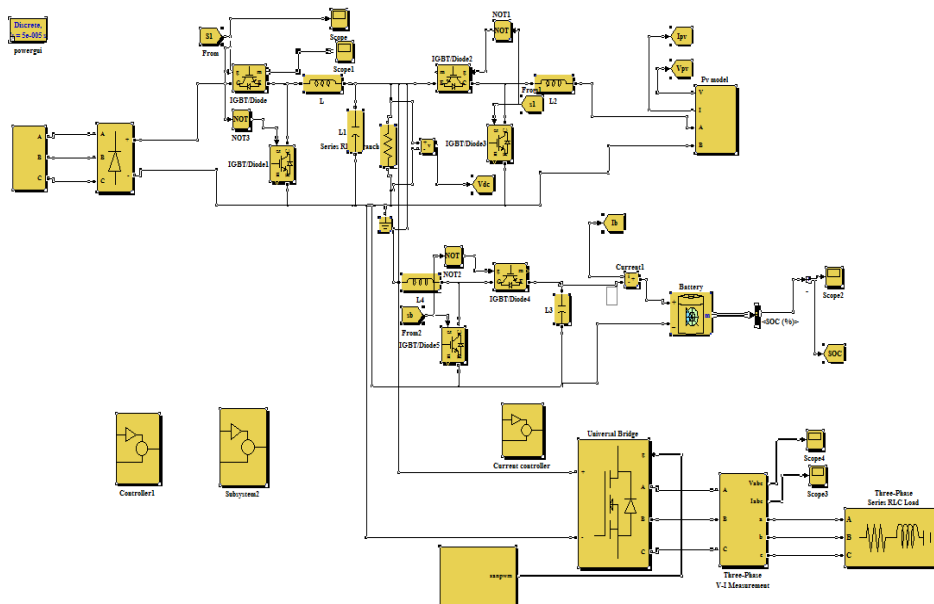


Fig.3. Proposed Matlab Circuit.

To evaluate the performance of the developed optimal EMS, Two test scenarios are carried out. They are

- 1.) Scenario I: Constant current charging mode.
- 2.) Scenario II: Constant voltage charging mode.

1) Scenario I: Constant Current Charging Mode:

This scenario covers the following three different cases which are run successively:

Case I: Wind turbine and PV array generate enough power at their MPPs to supply load demands and charge battery bank with its nominal charging current.

cost functions are defined as convex combinations of objectives with the weights $\beta_1 - \beta_4$. While β_1 and β_3 are close to 1.0, β_2 and β_4 are close to zero.

2) Box Constraints:

The below equation adds the pitch angle control feature to the developed EMS in order to limit the produced aerodynamic power by the wind turbine.

$$0 \leq -T_e \omega_r \leq P_{wt,nom} \quad (15)$$

The other box constraints on the manipulated variables and the system states are formulated as follows:

$$x_{min} \leq x \leq x_{max} \quad (16a)$$

$$u_{min} \leq u \leq u_{max} \quad (16b)$$

3) Initial Constraints:

Prior to calculating the optimal solution over the next receding horizon N , all system states, i.e., $[w_r, Q_{act}, I_f]^T$ as well as the dc bus voltage level are initialized by the measured or estimated values.

IV. SIMULATION AND RESULTS

A. Matlab Simulation Circuit:

Case II: The generated power is just enough to supply the load demands and therefore battery bank is not charged or is charged with the current less than its nominal charging current.

Case III: The generated power is more than the required power to supply the load demands and charge battery bank with its nominal charging current. Each case lasts for 5 minutes and therefore the total period of the simulation time is 15 minutes. In order to calculate the optimal control variables every 5 seconds, the developed NMPC controller runs exactly 60 times as per each case.

2) Scenario II: Constant voltage charging mode:

Terminal voltage of battery bank rises by Scenario II due to constant charging currents. Once the battery terminal voltage level reaches its gassing voltage, charging current should be gradually reduced in order to prevent exceeding gassing voltage threshold. This constant voltage charging strategy helps battery bank to be fully charged without the risk of permanent damage. From Fig. 5(a), it can be seen that the developed controller switches to the constant voltage charging mode when terminal voltage of battery bank reaches to its gassing voltage. For this purpose, the cost function of the developed NMPC strategy is switched as given in Step 3 of pseudo code of proposed optimal EMS as below.

Step 1: Configurations

Set $\bar{\alpha}_1 = 0.02 \bar{V}_{dc}$ and $\bar{\alpha}_2 = 0.01$;

Set $T_1 = 10.0$ (sec), $N=2$;

Instantiate an NLP solver;

Step 2: Measurements

Measure the states I_f , Q_{bat} and ω_r values from the system;

Measure the dc bus voltage V_{dc} .

Measure the battery stack voltage level V_{bstack} ;

Get the predicted wind speed, insolation, and load demand for the next 10 seconds from an external estimator;

Step 3: Constructing the OCP

If $V_{bstack} < V_{gas} N_{bats}$ THEN

Use Eq. (14a) as the cost function;

ELSE use Eq.(14b) as the cost function;

Construct the vector Φ (Eq.11b) using functionals

$f_1 - f_{24}$;

Apply the current and next step values of wind speed, insolation, and load demand as the OCP parameters;

Construct Eq. (11g) from the box constraints defined by the eqs. (15) and (16) as well as two constraints $|\alpha_1| \leq \bar{\alpha}_1$ and $|\alpha_2| \leq \bar{\alpha}_2$;

Step 4: Initializations

Set the measured values of I_f , Q_{bat} , and ω_r as the initial values of different states

Set the measured value of V_{dc} as the intial dc bus voltage value

Step 5: Discretization and solving the discretized problem

Discretize the OCP problem using the collection method

Construct equivalent NLP problem

Solve the equation NLP problem using standard NLP solvers to caluculate the optimal solution $\mathbf{u}^*(.)$;

Step 6: Applying the control variables

Constructing the control law using the first sample of the optimal solution i.e. $\mathbf{u}^*(.)$.

Apply the control law to the system

GOTO step 2: Measurements;

B. Matlab Simulation Results

1) Scenario I: Constant Current Charging Mode

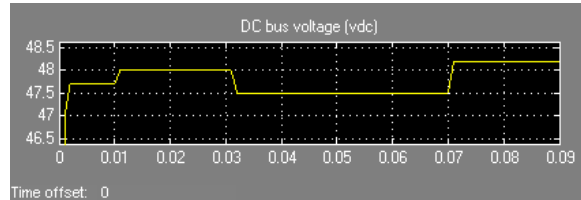


Fig.4 (a) Dc bus voltage

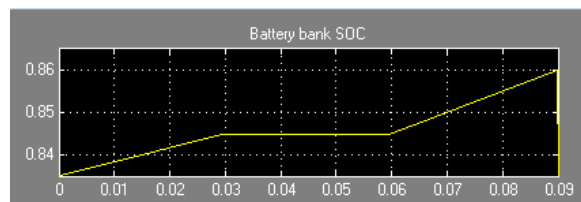


Fig.4 (b) Battery bank soc

From Fig. 4(a), it can be seen that after $t = 300$ s, when there is not enough generated power to charge battery, controller reduces the dc bus voltage level. However, at $t = 600$ s the voltage level returns back to the nominal value of 48.0 V. So the controller makes the dc bus voltage level within the permissible range i.e. 48.0 ± 0.96 V even when there is a significant change in load demand variations and change in wind speed which changes power generation from wind system. From Fig. 6(c), it can be seen that this strategy helps the battery to be charged up to high SOC values.

2) Scenario II: Constant voltage charging mode

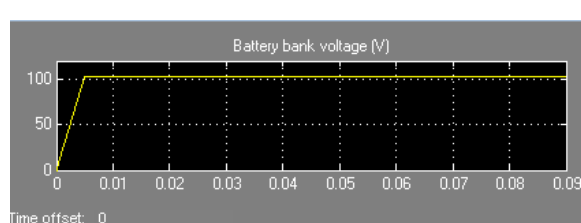


Fig.5 (a) Battery bank voltage

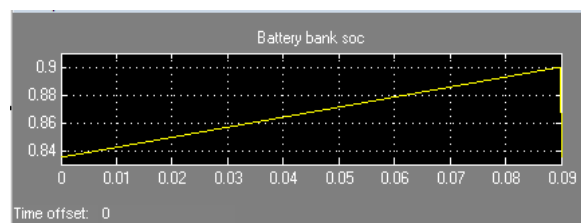


Fig.5 (b) Battery bank soc

From Fig. 5(a) it can be seen that the battery bank voltage reaches certain value i.e. a safe margin of the gassing voltage after some time and remains constant. This done by the controller which reduces the charging current gradually with respect to the safe margin of the gassing voltage in order to maintain the battery bank voltage constant. Fig. 5(b) indicates that the battery can be fully charged with the constant current-constant voltage regime with no risk of exceeding the gassing voltage.

3) Output of the inverter which supplies the ac load

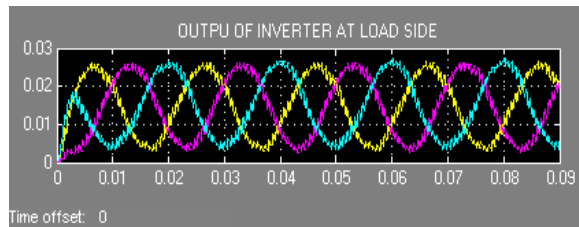


Fig. 6 output current of the inverter at load side

From the Fig. 6 it shows the 3-phase current output of the inverter which is used to supply the Ac dump loads at the standalone DC micro grid installed at the remote and rural areas. This output current is applied either directly to the loads or through a transformer depending upon the loads connected.

V. CONCLUSION

A coordinated and multivariable online NMPC strategy has been developed to address the optimal EMS, which deals with three main control objectives of standalone dc microgrids. These objectives are the voltage level regulation, proportional power sharing, and battery management. In order to address these objectives, the developed EMS simultaneously controls the pitch angle of the wind turbine and the switching duty cycles of three dc-dc converters. It has been shown that the developed controller tracks the MPPs of the wind and solar branches within the normal conditions and curtails their generations during the under load conditions. The provided flexible generation curtailment strategy realizes the constant current, constant voltage charging regime that potentially increases the life span of the battery bank. The simulation results have been shown its ability to achieve all control objectives.

REFERENCES

- [1] Arash M. Dizqah, Alireza Maher, Krishna Busawon, and Azadeh Kamjoo "A Multivariable Optimal Energy Management Strategy for Standalone DC Microgrids," IEEE transactions on power systems, vol. 30, no. 5, pp 2278-2287, September 2015.
- [2] R. S. Balog, W. W. Weaver, and P. T. Krein, "The load as an energy asset in a distributed DC smartgrid architecture," IEEE Trans. Smart Grid, vol. 3, no. 1, pp. 253–260, 2012.
- [3] J. M. Guerrero, M. Chandorkar, T. Lee, and P. C. Loh, "Advanced Control Architectures for Intelligent Microgrids-Part I: Decentralized and Hierarchical Control," IEEE Trans. Ind. Electron., vol. 60, no. 4, pp. 1254–1262, 2013.
- [4] S. Anand, B. G. Fernandes, and M. Guerrero, "Distributed control to ensure proportional load sharing and improve voltage regulation in low-voltage DC microgrids," IEEE Trans. Power Electro., vol. 28, no. 4, pp. 1900–1913, 2013.
- [5] Chen and L. Xu, "Autonomous DC voltage control of a DC microgrid with multiple slack terminals," IEEE Trans. Power Syst., vol. 27, no. 4, pp. 1897–1905, Nov. 2012.
- [6] Zhao, X. Zhang, J. Chen, C. Wang, and L. Guo, "Operation optimization of standalone microgrids considering lifetime characteristics of battery energy storage system," IEEE Trans. Sustain. Energy, Volume: 4, n0.4, pp: 934 - 943 Oct. 2013.
- [7] J. M. Guerrero, J. C. Vasquez, J. Matas, L. G. de Vicua, and M. Castilla, "Hierarchical control of droop-controlled AC and DC microgrids-a general approach toward standardization," IEEE Trans. Ind. Electron., vol. 58, no. 1, pp. 158–172, 2011.
- [8] P. H. Divshali, A. Alimardani, S. H. Hosseiniyan, and M. Abedi, "De-centralized cooperative control strategy of microsources for stabilizing autonomous VSC-Based microgrids," IEEE Trans. Power Syst., vol. 27, no. 4, pp. 1949–1959, Nov. 2012.
- [9] H. Fakham, D. Lu, and B. Francois, "Power control design of a battery charger in a hybrid active PV generator for load-following applications," IEEE Trans. Ind. Electron., vol. 58, no. 1, pp. 85–94, 2011.
- [10] X. Liu, P. Wang, and P. C. Loh, "A hybrid AC/DC microgrid and its co-ordination control," IEEE Trans. Smart Grid, vol. 2, no. 2, pp. 278–286, 2011.
- [11] Meharrar, M. Tioursi, M. Hatti, and A. B. Stambouli, "A variable speed wind generator maximum power tracking based on adaptative neuro-fuzzy inference system," Expert Syst. Applicat., vol. 38, no. 6, pp. 7659–7664, 2011.
- [12] O. Tremblay and L. Dessaint, "Experimental validation of a battery dynamic model for EV applications," World Elect. Vehicle Jornal., vol. 3, pp. 10–15, 2009
- [13] M. Dizqah, K. Busawon, and P. Fritzson, "Acausal modeling and simulation of the standalone solar power systems as hybrid DAEs," in Proc. 53rd Int. Conf. Scandinavian Simul. Soc., 2012.
- [14] N. Mohan, T. M. Undeland, and W. P. Robbins, Power Electronics: Converters, Applications, and Design. New York, NY, USA: Wiley, 1995.
- [15] J. H. Su, J. J. Chen, and D. S. Wu, "Learning Feedback Controller Design of Switching Converters Via MATLABSIMULINK," IEEE Transactions on Education, vol. 45, pp. 307–315, 2002.
- [16] L. Grüne and J. Pannek, "Nonlinear model predictive control: Theory and algorithms," in Communications and Control Engineering. New York, NY, USA: Springer, 2011.
- [17] R. Neidinger, "Introduction to automatic differentiation and MATLAB object-oriented programming," SIAM Rev., vol. 52, no. 3, pp. 545–563, 2010.

BIOGRAPHY



Manchem Sai Navesh is Pursuing M.Tech degree from Malla Reddy Engineering College (Autonomous), Hyderabad in the stream of control systems, completed B.Tech (EEE) from Swarandhra Engineering College, Narsapur in the year 2013. Areas of interests are Control Systems, Power System Operation and Control, Power System Analysis and Electrical Circuits.